PROCEEDINGS OF SCIENCE

Progress Toward Reproducing the GeV Galactic Center Excess Using CALET Data

Audrey R. Coleman,[a,*] **Wolfgang V. Zober,**[a] **Michela Negro,**[b] **Nicholas W. Cannady**[c] **and Brian F. Rauch**[a] **and the CALET collaboration**

[a] *Department of Physics and McDonnell Center for the Space Sciences, Washington University in St Louis, St Louis, MO 63130, USA*

[b] *Department of Physics and Astronomy, Louisiana State University, Baton Rouge, LA 70803 USA*

[c] *Astroparticle Physics Laboratory, NASA/GSFC, Greenbelt, Maryland 20771, USA*

E-mail: audrey.c@wustl.edu

The Calorimetric Electron Telescope (CALET) currently has more than nine years of high-energy γ-ray data that has not been fully explored. A region of particular interest for γ-ray astronomy is the Galactic Center (GC). Analysis of Fermi Large Area Telescope (LAT) data shows an excess of GeV γ rays from the GC region that could possibly be explained by the annihilation of weakly interacting massive particles (WIMPs) or an unresolved population of millisecond pulsars. Here we present the analysis of the Crab and Geminga using `FermiPy` and progress toward analysis of the Galactic Center using CALET data.

39th International Cosmic Ray Conference (ICRC2025)
15–24 July 2025
Geneva, Switzerland

*Speaker

PoS(ICRC2025)613

1. Introduction

The CALorimetric Electron Telescope (CALET) was launched and installed on the International Space Station (ISS) Japanese Experiment Module - Exposed Facility (JEM-EF) in August 2015. It has been taking scientific data since October 2015. CALET's primary science goal is to discover nearby cosmic-ray accelerators and to search for dark matter by measuring all-electron (electrons and positrons) and gamma-ray spectra in the range of 1 GeV to 1 TeV.

Previous work [1, 2] has shown that CALET gamma-ray spectra for the Crab, Geminga, and Vela are consistent with those observed by Fermi-LAT. This work describes our progress in integrating CALET gamma-ray data analysis into `FermiPy` [3] to take advantage of this powerful, well-tested, and publicly available software. One goal is to use `FermiPy` to determine the presence of the Galactic Center Excess (GCE) [4] in CALET data. Using `FermiPy` for a CALET GCE analysis will allow us to make use of LAT catalogs and diffuse models provided by the package, as well as to directly compare our results with the Fermi-LAT GCE spectra produced using `FermiPy` (see [5, 6] for Fermi-LAT GCE analyses that explicitly use `FermiPy`). Cross-correlation between independent data sets may reveal subthreshold sources such as millisecond pulsars, which are a proposed explanation of the GCE, which are currently obscured by noise. This noise would not correlate between the data sets.

2. CALET Detector

CALET consists of two instruments: the Calorimeter (CAL) and the CALET Gamma-ray Burst Monitor (CGBM). The CAL is the main instrument and is the one used in this work. It has a field of view (FOV) of ~45° from the zenith and can observe high-energy electrons from ~1 GeV to ~20 TeV, protons, helium, and heavy nuclei from ~ 10 GeV to 1000 TeV and gamma-rays from ~1 GeV to ~10 TeV. The CAL is made up of three components: the Charge Detector (CHD), the Imaging Calorimeter (IMC), and the Total Absorption Calorimeter (TASC). The CHD is located above the IMC and measures the charge of the incident particle. The IMC reconstructs the track of the incident particle and finely images the initial shower development. The TASC absorbs the entire energy of the incoming particle and is able to identify the particle type. The CAL has two gamma-ray trigger modes: a low-energy gamma-ray (LE-γ) mode with a threshold of ~1 GeV which is activated when the geomagnetic latitude is below 20°, and a high-energy (HE) mode which is always on and has a threshold of ~10 GeV. Further details on the CAL detector and triggers can be found in [7].

3. CALET Gamma-ray Analysis

The CAL gamma-ray performance and initial CAL gamma-ray results for steady sources are described in detail in Ref. [1]. At 10 GeV, the energy and angular resolutions are estimated to be 3% and 0.4°, respectively. The energy dependence of the energy resolution is shown in Fig. 1. CAL's thick calorimeter allows for good performance into the high-energy region.

The CAL point spread function (PSF) and effective area are described in Ref. [1]. The CAL PSF roughly follows the treatment of the Fermi-LAT PSF presented in Ref. [10]. The PSF of CAL is best fitted by a pair of King functions that represent a core and tail contribution. The maximum

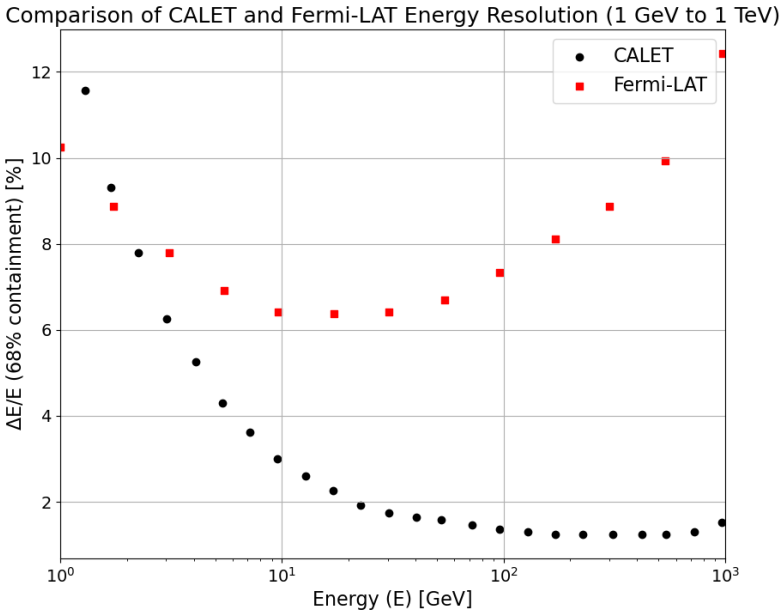

Figure 1: Energy resolution as a function of energy for CALET (including calibration errors) and Fermi-LAT (Pass 8 P8R3_SOURCE_V3). CALET data courtesy of Ref. [8], Fermi-LAT data courtesy of Ref. [9]

effective area is approximately 400 cm^2 and sees no counts above an inclination angle of ~45° due to the FOV cut. The CAL effective areas for various incident angles are shown compared to Fermi-LAT in Fig. 2 as a function of energy.

4. Integration with FermiPy

`FermiPy` is a Python package that automates Fermitools analyses. The setup tool housed in the GTAnalysis module will be the primary focus of this work. The `gta.setup()` tool runs pre-processing for each component of the analysis and constructs a joint likelihood object. It performs the tasks of data selection, data binning, and model generation and produces a counts cube for the ROI, an all-sky exposure cube, an all-sky livetime cube, and a source map cube containing maps for each of the components in the ROI after convolution with exposure and the PSF.

CALET data are pre-processed before analysis, rendering many of these steps unnecessary and incompatible with the CALET data format. The counts, exposure, and livetime cubes generated by this routine can be created through a CALET-specific pipeline that accounts for the differences between Fermi-LAT and CALET data. Doing so takes advantage of the fact that `gta.setup()` will not generate files that already exist in the working directory and will thus skip the steps of generating counts, exposure, and livetime cubes. It will then use these CALET data cubes, along with a CALET instrument response function, to generate the source map cube. At this point the CALET data will be in the format expected by `FermiPy` and it will be possible to use `FermiPy` for CALET data analysis.

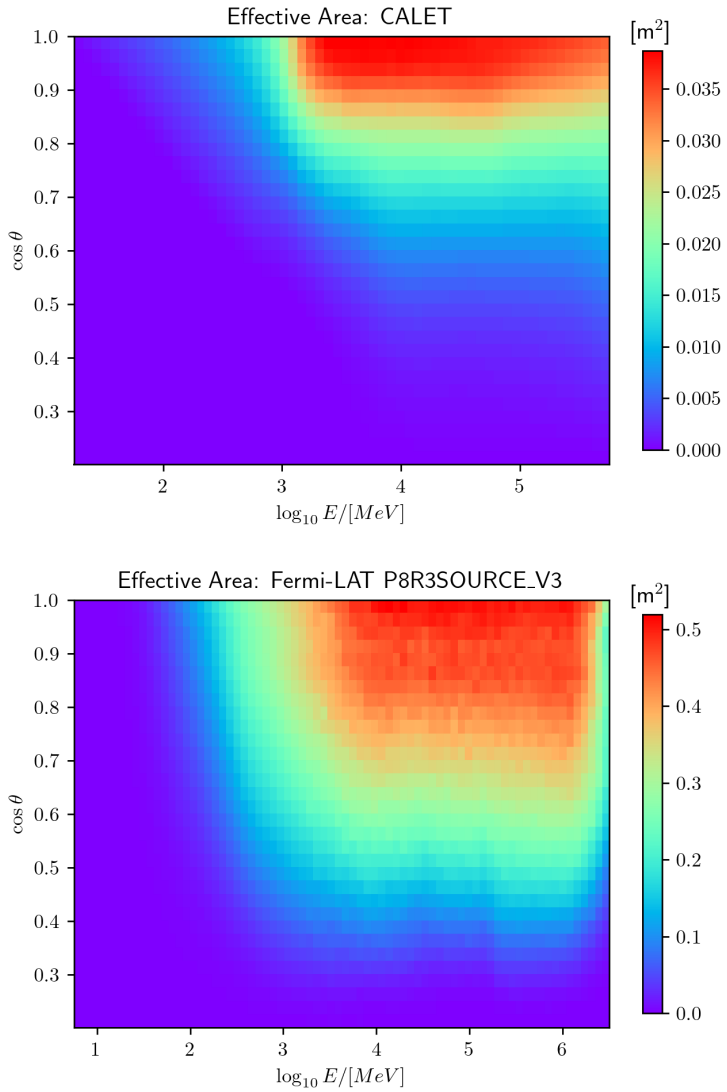

Figure 2: Effective areas as a function of energy and inclination angle (θ) for CAL (Top) and Fermi-LAT (Bottom). The CAL LE-γ trigger turns on at 10^3 MeV.

To make the counts cube, we apply these energy and ROI cuts to the CALET data and generate 2D histograms with the same 0.1° binning. A histogram is generated for each energy bin. The arrays describing these histograms are saved as a FITS PrimaryHDU. The counts cube requires two extensions, containing the energy bin edges and Good Time Intervals (GTIs). The counts cubes generated using Fermi-LAT data give the bin edges in units of keV, which we replicated for our CALET counts cube. The GTIs describe time ranges in which the Fermi-LAT data can be considered valid. Since CALET event validation takes place before the construction of the counts cube, we use a single GTI that spans the entire time range under analysis.

To generate the exposure cube we take the CALET exposures, which are in HEALpix format, and map them to Galactic coordinates. We then interpolate to match the energy bins used by

Fermi-LAT for a more direct comparison. We use the same energy bin edges (in MeV) and the single GTI described previously.

The CALET instrument response functions (IRFs) were made by duplicating the framework of a Fermi-LAT IRF and substituting CALET values where appropriate. For the PSF, CALET does not currently differentiate event quartiles, so only one constant PSF is used. Our energy dispersion is treated as a constant. The effective area is binned to match Fermi-LAT to streamline the analysis. Additionally, the CALET IRFs currently lack the ability to differentiate events by FRONT or BACK of the detector, so the same files are used for each. In future work, we will enhance the IRF to differentiate based on the location of shower development within the IMC. These custom IRFs were then added to the `Fermitools` directory structure, allowing them to be called by `FermiPy`.

`FermiPy` uses the livetime cube to speed up the exposure calculations and is used to generate a source model. Through private communication with members of the Fermi-LAT collaboration familiar with the `FermiPy` code we know that the livetime cube only provides the sky binning for the source model. Since CALET provides the software with an exposure cube, a livetime cube is only needed for source model generation. As such, we use the livetime cube generated using Fermi-LAT data, which matches the CALET sky binning and does not require us to create a new livetime cube.

5. Results

We run `gta.setup()` using Fermi-LAT data for the Crab and Geminga and follow the format of the generated files to construct the CALET data cubes. We select photon data belonging to the Pass 8 SOURCE event class and the corresponding IRFs (P8R3_SOURCE_V3). We select data of event type 3 in the energy range of 1-10 GeV for the Crab and 2-20 GeV for Geminga over the time range of 2015 October 01 to 2022 December 31, which spans the entirety of CALET's processed data. The remaining two years of data are currently being processed and will be included in our analysis when they become available. For this analysis, we use an ROI width of 15°, a bin size of 0.1, and 6 bins per energy decade. We use the same data selection for the CALET data and use CALET IRFs. CAL LE-γ data are used for this analysis. For both the Fermi-LAT and CALET analyses we use the publicly available Galactic diffuse emission model gll_iem_v07 and use the 4FGL-DR3 catalog [11] for our model.

We perform a simple fit of both sources to establish how CAL compares to Fermi-LAT. Note that the following analysis of the Crab will not match published Fermi-LAT results, which consider the Crab pulsar, the synchrotron emission of the nebula, and the inverse Compton emission of the nebula together. Here we only consider the pulsar for simplicity, as the intent of this first fit is to establish that CAL data are being read into `FermiPy` correctly. We free the normalization of all sources within 3° of the ROI center. We also free all parameters of the isotropic and galactic diffuse components as well as the source under study. We then run `gta.fit()`, which returns the best-fit spectral energy distribution (SED) parameters and the full covariance matrix.

After running `gta.fit()`, the command `gta.write_roi()` produces several diagnostic plots, which include counts maps and plots showing the offset of the data from the source position in Galactic coordinates. Fig. 3 shows counts maps for the Crab and Geminga. Fig.s 4a and 4b show the offsets in Galactic latitude and longitude of the data from the source position. In both figures

there is good agreement between the data and the expected distribution generated by `FermiPy` using the CALET IRF.

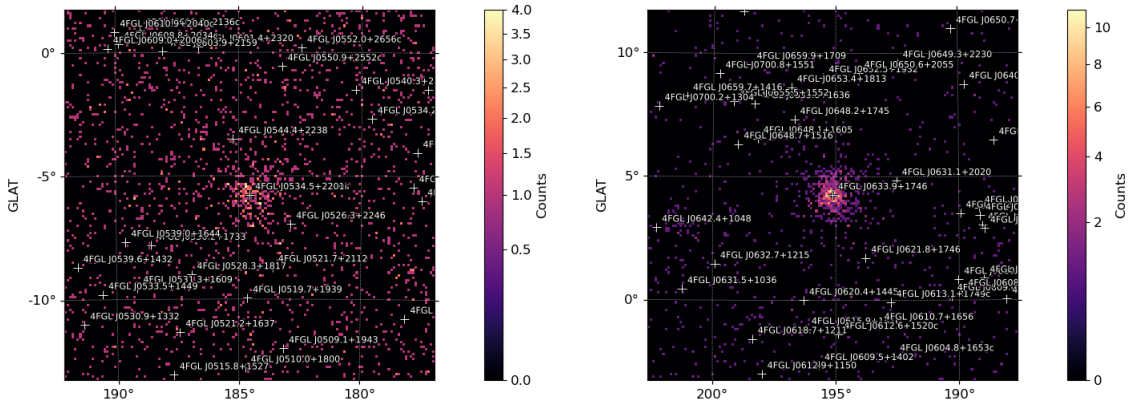

Figure 3: Counts maps for the Crab (Left) and Geminga (Right) produced using CALET data with FermiPy. Crosses indicate source positions in the 4FGL DR3 catalog.

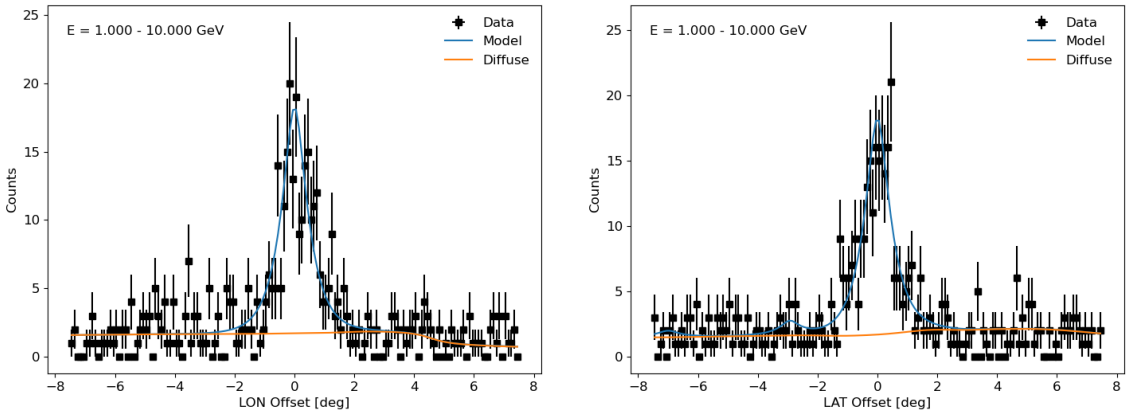

Figure 4(a): Offsets of CAL data from the Crab source position in Galactic longitude (Left) and Galactic latitude (Right). Included also are lines representing the model of the source as well as the Galactic diffuse emission.

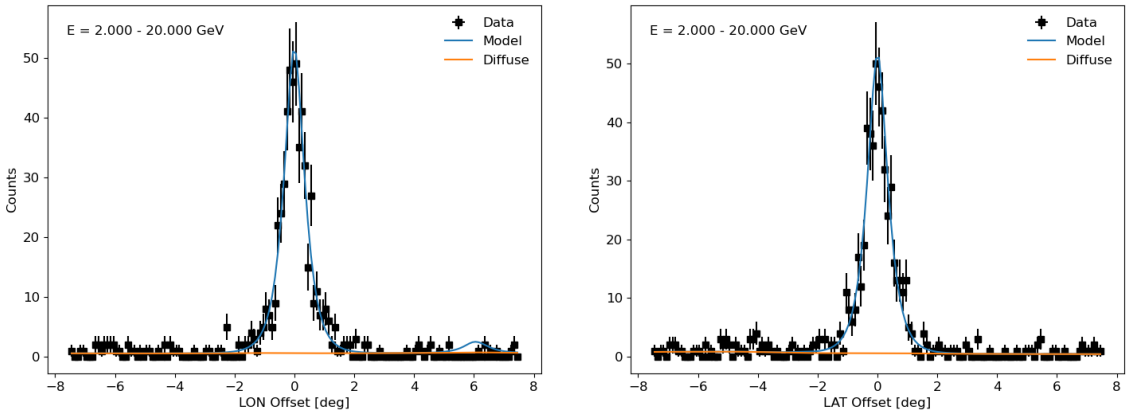

Figure 4(b): Offsets of CAL data from the Geminga source position in Galactic longitude (Left) and Galactic latitude (Right). Included also are lines representing the model of the source as well as the Galactic diffuse emission.

Finally, we generate SEDs for the two sources using `gta.sed`, the results of which are shown

in Fig. 5. Also shown are Fermi-LAT SEDs for the Crab and Geminga generated using the analysis pipeline described previously. The Crab and Geminga SEDs show good agreement between CALET and Fermi-LAT. Above 10 GeV the efficiency of the LE-γ trigger decreases, resulting in larger error bars on the final point in the Geminga SED. Future work will use data from the HE trigger above 10 GeV.

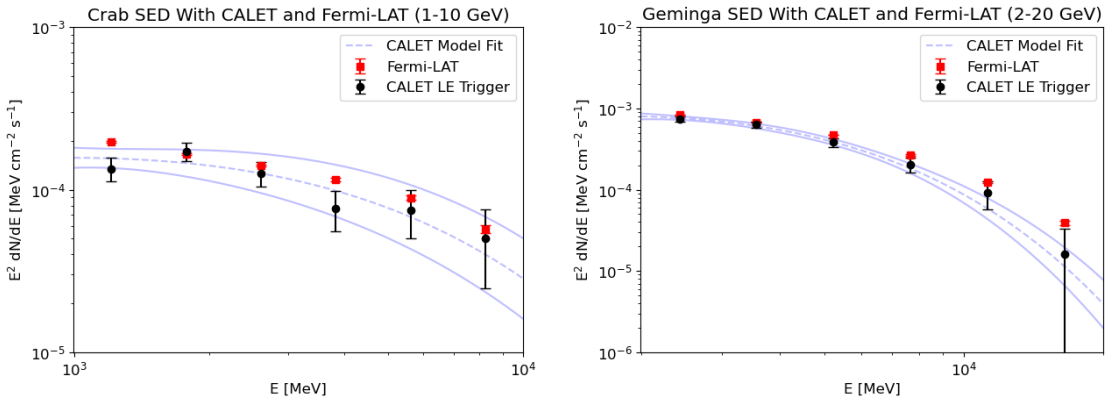

Figure 5: SEDs for the Crab (Left) and Geminga (Right) produced using CALET data with FermiPy. Fermi-LAT data included for comparison.

Acknowledgments We gratefully acknowledge Alex Reustle and Joseph Asercion for their help in understanding how `FermiPy` functions and how the various data cubes are used by the software. We gratefully acknowledge JAXA's contributions to the development of CALET and to the operations aboard the JEM-EF on the ISS. This work was supported in part by JSPS Grant-in-Aid for Scientific Research (S) No. 26220708, No. 19H05608, and No. 24H00025, JSPS Grant-in-Aid for Scientific Research (B) No. 24K00665, and by the MEXT Supported Program for the Strategic Research Foundation at Private Universities (2011-2015) (No. S1101021) at Waseda University. The CALET effort in Italy is supported by ASI under Agreement No. 2013-018-R.0 and its amendments. The CALET effort in the United States is supported by NASA through Grants No. NNX16AB99G, No. NNX16AC02G, and No. NNH14ZDA001N-APRA-0075.

6. Bibliography

[1] N. Cannady et al. Characteristics and Performance of the CALorimetric Electron Telescope (CALET) Calorimeter for Gamma-Ray Observations. *Astrophys. J. Suppl.*, 238(5), 2018.

[2] M. Mori and N. Cannady for the CALET Collaboration. Results from CALorimetric Electron Telescope (CALET) Observations of Gamma-rays on the International Space Station. *PoS (ICRC2023)*, 708.

[3] M. Wood, R. Caputo, E. Charles, M. Di Mauro, J. Magill, J.S. Perkins. Fermipy: An open-source Python package for analysis of Fermi-LAT Data. *PoS (ICRC2017)*, 301:824.

[4] D. Hooper and L. Goodenough. Dark Matter Annihilation in the Galactic Center as seen by the Fermi Gamma Ray Space Telescope. *Physics Letters B*, 697(5):412–428, 2011.

[5] M. Ackermann et al. The Fermi Galactic Center GeV Excess and Implications for Dark Matter. *Astrophys. J.*, 840(43), 2017.

[6] M. Di Mauro. Characteristics of the Galactic Center excess measured with 11 years of Fermi-LAT data. *Physical Review D*, 103(6), 2021.

[7] Y. Asaoka et al. On-orbit operations and offline data processing of CALET onboard the ISS. *Astropart.Phys.*, 100:29–37, 2018.

[8] Y. Asaoka et al. Energy Calibration of CALET onboard the International Space Station. *Astroparticle Physics*, 91:1–10, 2017.

[9] Fermi-lat performance. https://www.slac.stanford.edu/exp/glast/groups/canda/lat_ Performance.htm.

[10] M. Ackermann et al. The fermi large area telescope on orbit: event classification, instrument response functions, and calibration. *Astrophys. J. Suppl.*, 203(4), 2012.

[11] S. Abdollahi et al. Incremental Fermi Large Area Telescope Fourth Source Catalog. *Astrophys. J. Suppl.*, 260(2):53, 2022.

Full Author List: CALET Collaboration

O. Adriani,[1,2] Y. Akaike,[3,4] K. Asano,[5] Y. Asaoka,[5] E. Berti,[2,6] P. Betti,[2,6] G. Bigongiari,[7,8] W.R. Binns,[9] M. Bongi,[1,2] P. Brogi,[7,8] A. Bruno,[10] N. Cannady,[11] G. Castellini,[6] C. Checchia,[7,8] M.L. Cherry,[12] G. Collazuol,[13,14] G.A. de Nolfo,[10] K. Ebisawa,[15] A. W. Ficklin,[12] H. Fuke,[15] S. Gonzi,[1,2,6] T.G. Guzik,[12] T. Hams,[16] K. Hibino,[17] M. Ichimura,[18] M.H. Israel,[9] K. Kasahara,[19] J. Kataoka,[20] R. Kataoka,[21] Y. Katayose,[22] C. Kato,[23] N. Kawanaka,[24,25] Y. Kawakubo,[26] K. Kobayashi,[3,4] K. Kohri,[25,27] H.S. Krawczynski,[9] J.F. Krizmanic,[11] P. Maestro,[7,8] P.S. Marrocchesi,[7,8] M. Mattiazzi,[13,14] A.M. Messineo,[8,28] J.W. Mitchell,[11] S. Miyake,[29] A.A. Moiseev,[11,30,31] M. Mori,[32] N. Mori,[2] H.M. Motz,[33] K. Munakata,[23] S. Nakahira,[15] J. Nishimura,[15] M. Negro,[12] S. Okuno,[17] J.F. Ormes,[34] S. Ozawa,[35] L. Pacini,[2,6] P. Papini,[2] B.F. Rauch,[9] S.B. Ricciarini,[2,6] K. Sakai,[36] T. Sakamoto,[26] M. Sasaki,[11,30,31] Y. Shimizu,[17] A. Shiomi,[37] P. Spillantini,[1] F. Stolzi,[7,8] S. Sugita,[26] A. Sulaj,[7,8] M. Takita,[5] T. Tamura,[17] T. Terasawa,[5] S. Torii,[3] Y. Tsunesada,[38,39] Y. Uchihori,[40] E. Vannuccini,[2] J.P. Wefel,[12] K. Yamaoka,[41] S. Yanagita,[42] A. Yoshida,[26] K. Yoshida,[19] and W. V. Zober[9]

[1]Department of Physics, University of Florence, Via Sansone, 1 - 50019, Sesto Fiorentino, Italy [2]INFN Sezione di Firenze, Via Sansone, 1 - 50019, Sesto Fiorentino, Italy [3]Waseda Research Institute for Science and Engineering, Waseda University, 17 Kikuicho, Shinjuku, Tokyo 162-0044, Japan [4]Space Environment Utilization Center, Human Spaceflight Technology Directorate, Japan Aerospace Exploration Agency, 2-1-1 Sengen, Tsukuba, Ibaraki 305-8505, Japan [5]Institute for Cosmic Ray Research, The University of Tokyo, 5-1-5 Kashiwa-no-Ha, Kashiwa, Chiba 277-8582, Japan [6]Institute of Applied Physics (IFAC), National Research Council (CNR), Via Madonna del Piano, 10, 50019, Sesto Fiorentino, Italy [7]Department of Physical Sciences, Earth and Environment, University of Siena, via Roma 56, 53100 Siena, Italy [8]INFN Sezione di Pisa, Polo Fibonacci, Largo B. Pontecorvo, 3 - 56127 Pisa, Italy [9]Department of Physics and McDonnell Center for the Space Sciences, Washington University, One Brookings Drive, St. Louis, Missouri 63130-4899, USA [10]Heliospheric Physics Laboratory, NASA/GSFC, Greenbelt, Maryland 20771, USA [11]Astroparticle Physics Laboratory, NASA/GSFC, Greenbelt, Maryland 20771, USA [12]Department of Physics and Astronomy, Louisiana State University, 202 Nicholson Hall, Baton Rouge, Louisiana 70803, USA [13]Department of Physics and Astronomy, University of Padova, Via Marzolo, 8, 35131 Padova, Italy [14]INFN Sezione di Padova, Via Marzolo, 8, 35131 Padova, Italy [15]Institute of Space and Astronautical Science, Japan Aerospace Exploration Agency, 3-1-1 Yoshinodai, Chuo, Sagamihara, Kanagawa 252-5210, Japan [16]Center for Space Sciences and Technology, University of Maryland, Baltimore County, 1000 Hilltop Circle, Baltimore, Maryland 21250, USA [17]Kanagawa University, 3-27-1 Rokkakubashi, Kanagawa, Yokohama, Kanagawa 221-8686, Japan [18]Faculty of Science and Technology, Graduate School of Science and Technology, Hirosaki University, 3, Bunkyo, Hirosaki, Aomori 036-8561, Japan [19]Department of Electronic Information Systems, Shibaura Institute of Technology, 307 Fukasaku, Minuma, Saitama 337-8570, Japan [20]School of Advanced Science and Engineering, Waseda University, 3-4-1 Okubo, Shinjuku, Tokyo 169-8555, Japan [21]Okinawa Institute of Science and Technology, 1919-1 Tancha, Onna-son, Kunigami-gun Okinawa 904-0495, Japan [22]Faculty of Engineering, Division of Intelligent Systems Engineering, Yokohama National University, 79-5 Tokiwadai, Hodogaya, Yokohama 240-8501, Japan [23]Faculty of Science, Shinshu University, 3-1-1 Asahi, Matsumoto, Nagano 390-8621, Japan [24]Department of Physics, Graduate School of Science, Tokyo Metropolitan University , 1-1 Minamii-Osawa, Hachioji, Tokyo 192-0397, Japan [25]National Astronomical Observatory of Japan, 2-21-1 Osawa, Mitaka, Tokyo 181-8588, Japan [26]Department of Physical Sciences, College of Science and Engineering, Aoyama Gakuin University, 5-10-1 Fuchinobe, Chuo, Sagamihara, Kanagawa 252-5258, Japan [27]Institute of Particle and Nuclear Studies, High Energy Accelerator Research Organization, 1-1 Oho, Tsukuba, Ibaraki 305-0801, Japan [28]University of Pisa, Polo Fibonacci, Largo B. Pontecorvo, 3 - 56127 Pisa, Italy [29]Department of Electrical and Computer Engineering, National Institute of Technology (KOSEN), Gifu College, 2236-2 Kamimakuwa, Motosu-city, Gifu 501-0495, Japan [30]Center for Research and Exploration in Space Sciences and Technology, NASA/GSFC, Greenbelt, Maryland 20771, USA [31]Department of Astronomy, University of Maryland, College Park, Maryland 20742, USA [32]Department of Physical Sciences, College of Science and Engineering, Ritsumeikan University, Shiga 525-8577, Japan [33]Faculty of Science and Engineering, Global Center for Science and Engineering, Waseda University, 3-4-1 Okubo, Shinjuku, Tokyo 169-8555, Japan [34]Department of Physics and Astronomy, University of Denver, Physics Building, Room 211, 2112 East Wesley Avenue, Denver, Colorado 80208-6900, USA [35]Quantum ICT Advanced Development Center, National Institute of Information and Communications Technology, 4-2-1 Nukui-Kitamachi, Koganei, Tokyo 184-8795, Japan [36]Kavli Institute for Cosmological Physics, The University of Chicago, 5640 South Ellis Avenue, Chicago, IL 60637, USA [37]College of Industrial Technology, Nihon University, 1-2-1 Izumi, Narashino, Chiba 275-8575, Japan [38]Graduate School of Science, Osaka Metropolitan University, Sugimoto, Sumiyoshi, Osaka 558-8585, Japan [39]Nambu Yoichiro Institute for Theoretical and Experimental Physics, Osaka Metropolitan University, Sugimoto, Sumiyoshi, Osaka 558-8585, Japan [40]National Institutes for Quantum and Radiation Science and Technology, 4-9-1 Anagawa, Inage, Chiba 263-8555, Japan [41]Nagoya University, Furo, Chikusa, Nagoya 464-8601, Japan [42]College of Science, Ibaraki University, 2-1-1 Bunkyo, Mito, Ibaraki 310-8512, Japan

PoS(ICRC2025)613